Article:
Michoud, V, Hansen, RF, Locoge, N et al. (2 more authors) (2015) Detailed characterizations of the new Mines Douai comparative reactivity method instrument via laboratory experiments and modeling. Atmospheric Measurement Techniques, 8 (8). pp. 3537-3553. ISSN 1867-1381

https://doi.org/10.5194/amt-8-3537-2015

Supplementary materials to :

Detailed characterizations of the new Mines Douai Comparative Reactivity Method instrument via laboratory experiments and modeling

V. Michoud[1], R. F. Hansen[1,2,3,*], N. Locoge[1], P. S. Stevens[2,3], S. Dusanter[1,2].

[1] Mines Douai, SAGE, F-59508, Douai, France

[2] School of Public and Environmental Affairs, Indiana University, Bloomington, IN, USA

[3] Department of chemistry, Indiana University, Bloomington, IN, USA

Correspondence to: Sebastien Dusanter (sebastien.dusanter@mines-douai .fr) and Vincent Michoud (Vincent.michoud@mines-douai.fr)

*now at: school of chemistry, University of Leeds, Leeds, UK

Supplementary material 1: Comparison between measured and calculated total OH reactivity values for two different gas mixtures: Non-Methane Hydrocarbons (NMHCs) and Oxygenated VOCs (OVOCs)

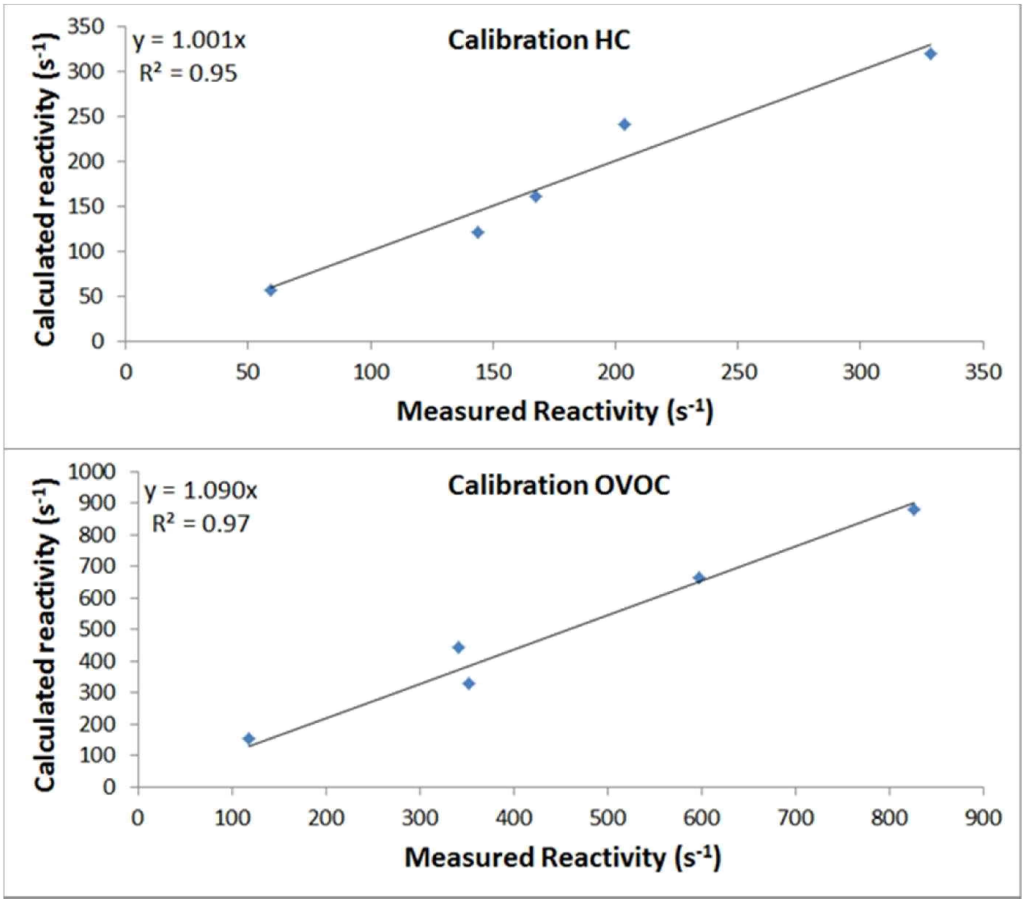

Figure S1: Scatter plot of calculated-to-measured OH reactivity for two different gas mixtures: NMHCs (top panel) and OVOCs (bottom panel) at pyrrole to OH ratios of 1.9 and 1.8, respectively. Chemical compositions of these mixtures are given in table S1. The measured OH reactivity corresponds to the total OH reactivity measured by MD-CRM and corrected for changes in humidity between C2 and C3 and for not operating the instrument under pseudo first order conditions. Correction for dilution is not performed since it is accounted for in the calculated OH reactivity.

Table S1: Chemical composition of the OVOC and NMHC mixtures.

Species OVOC mixture	Mixing ratios (ppm)	Species NMHC mixture	Mixing ratios (ppm)
Methanol	2.15	Acetonitrile	0.63
Acetaldehyde	1.43	Acrylonitrile	0.51
Acetone	4.50	Benzene	0.96
Methyl Ethyl Ketone	1.40	Toluene	0.91
2-Methylfuran	1.51	EthylBenzene	0.80
Acrolein	1.48	1,2,4-TrimethylBenzene	0.52
Methacrolein	1.65	Styrene	0.71
Methyl Vinyl Ketone	1.54	Alpha-Pinene	1.07
3-Methyl-2-buten-1-ol	0.60	Methyl Sulfur	1.14

Table S2: Reactions included in the simple mechanism (see section 3.1 of the main manuscript).

Reactions	Bimolecular rate constants (cm^3 $molecules^{-1}$ s^{-1})
$H + O_2 = HO_2$	$7.5x10^{-11}$
$OH + VOC = RO_2$	$5.0x10^{-12}$
$OH + Pyrrole = RO_2$	$1.2x10^{-10}$
$^{*}RO_2 + RO_2 =$	$3.4x10^{-13}$
$^{*}RO_2 + HO_2 =$	$5.2x10^{-12}$
$RO_2 + NO = RO+NO_2$	$7.7x10^{-12}$
$RO + O_2 = HO_2$	$1.9x10^{-15}$

* the formation of a product is not accounted for in the mechanism

In addition to the reactions shown in Table S2, inorganic reactions from IUPAC 2001 have been added in the mechanism, leading to a total of 42 reactions.

Supplementary material 2: Experiments performed to investigate the NO artifact in the presence of VOC reactivity – addition of ethane and isoprene

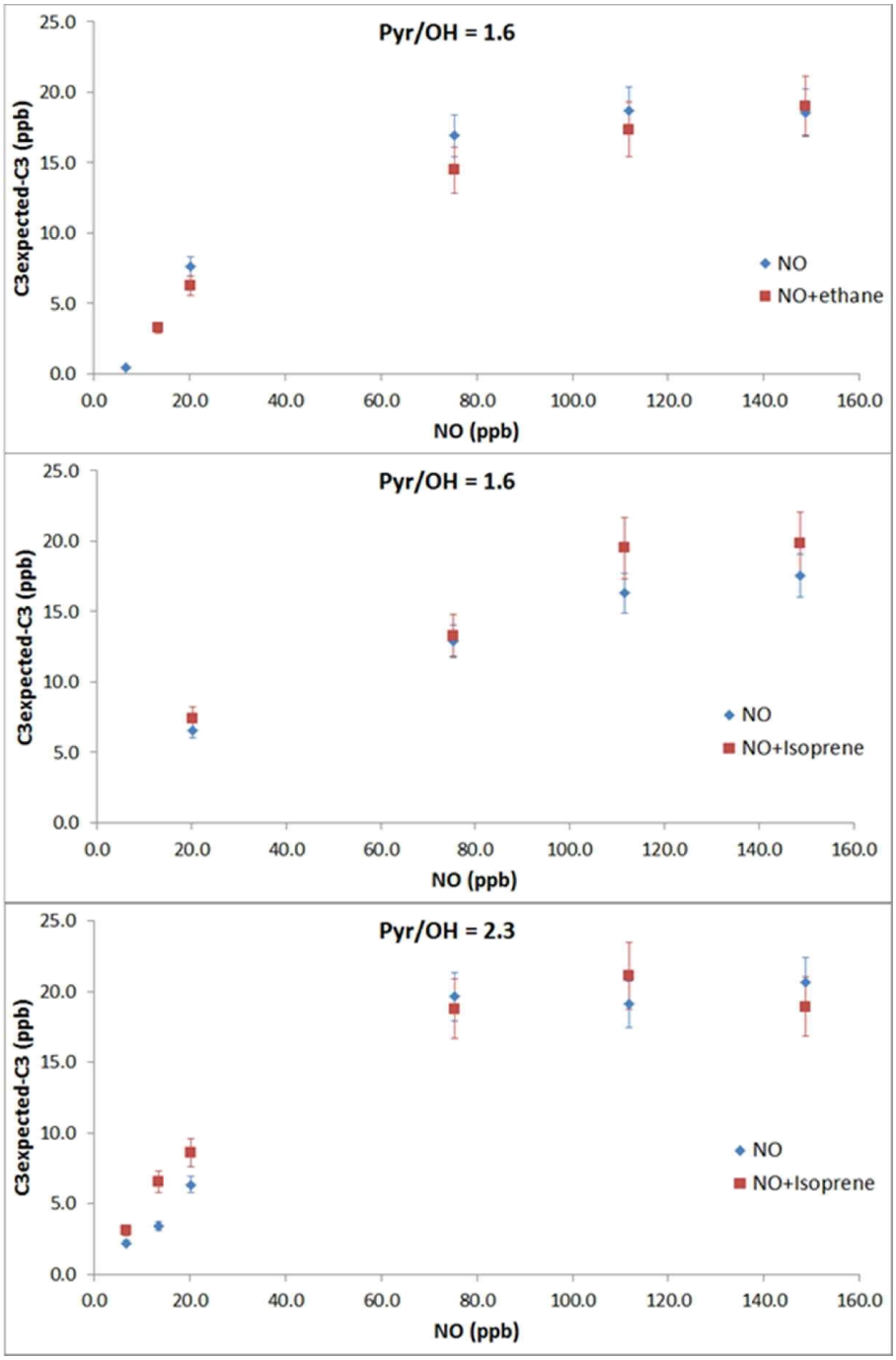

Figure S2: Changes in C3 (ΔC3 = C3 expected – C3 measured) as a function of NO in the reactor with (red) and without (blue) addition of a VOC. These experiments have been conducted using two different standards (ethane and isoprene) selected for their different kinetic rate constants with OH (2.4 10^{-13} and 1.0 10^{-10} cm^3 $molecules^{-1}$ s^{-1}, respectively). The concentrations added were 3.7 ppm and 14.6 ppb for ethane and isoprene, respectively, leading to calculated OH reactivity values of 22.2 and 36.6 s^{-1}, respectively. Experiments

made using isoprene have been conducted at two different Pyrrole-to-OH ratios (1.6 and 2.3) to test the influence of this parameter on the NO artifact in the presence of a VOC.

Differences observed in the NO artifact when VOCs are added in the reactor are within experimental uncertainties (9-11%), except when NO is low during the isoprene experiment made at a pyrrole-to-OH ratio of 2.3. No clear influence of the Pyrrole-to-OH ratio or of the VOC reactivity has been found on the amplitude of the NO artifact.

Supplementary material 3: Comparison between real and apparent Pyrrole-to-OH ratios

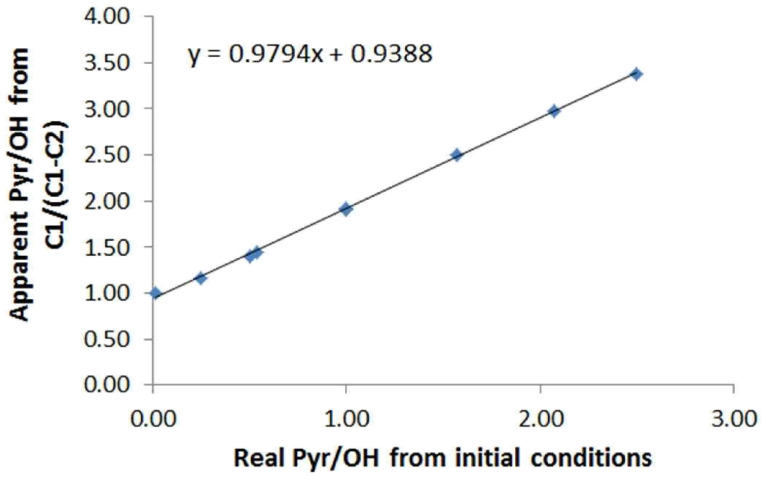

Figure S3: Comparison between real and apparent pyrrole-to-OH ratios for simulations conducted under dry conditions with the simple mechanism presented in section 3.1 of the main manuscript. Apparent pyrrole-to-OH ratios are calculated using Eq. (2), where C1 is the initial concentration of pyrrole and C2 the final concentration when OH has been fully reacted in the simulations. This apparent ratio provides the amount of OH that has reacted with pyrrole.

This figure shows that running the CRM instrument at an apparent pyrrole-to-OH ratio of 1.5-2.5 leads to a real ratio of approximately 0.5-1.5. The main manuscript and this supplementary material always refer to the apparent pyrrole-to-OH ratio since it is the measurable quantity.

Supplementary material 4: Experimental measurements of the OH mixing ratio inside the CRM reactor

Experiments were conducted to determine the OH mixing ratio inside the reactor. A large amount of isoprene (3 ppm) was injected inside the reactor in absence of pyrrole with (mercury lamp ON) or without (mercury lamp OFF) OH production. Isoprene was monitored by the PTR-ToFMS instrument at m/z 69. Simulations were conducted using MCM to ensure that this level of isoprene allows scavenging more than 97% of OH in the reactor. The OH mixing ratio present within the reactor can be derived from the decrease of isoprene when the OH production is turned ON. This OH mixing ratio, referred as “OH experiment”, was

determined at two different pyrrole-to-OH ratios of 1.6 and 3.8. The level of OH quantified experimentally from (C1-C2), i.e. the amount of OH reacting with pyrrole, is referred as "OH estimated CRM" and is compared to the total mixing ratio of OH determined experimentally. In addition, the OH mixing ratio necessary to reproduce the experimental C1-C2 modulation with the model is referred as "OH model". The three OH mixing ratios are shown in Fig. S4.

As seen in this figure, OH experiment is higher than the level determined from the C1-C2 modulation but only slightly lower (~10-20%) than OH model (within experimental uncertainties). However, the amount of isoprene injected inside the reactor may not be high enough to scavenge all the OH radicals if a segregation occurs between the reactants (see supplementary material S8). Some OH might still react with HO_2, leading to a slight underestimation of OH experiments. From these results, we consider that OH mixing ratios set in the model to simulate the experimental C1-C2 modulations are representative of the real mixing ratio in the reactor.

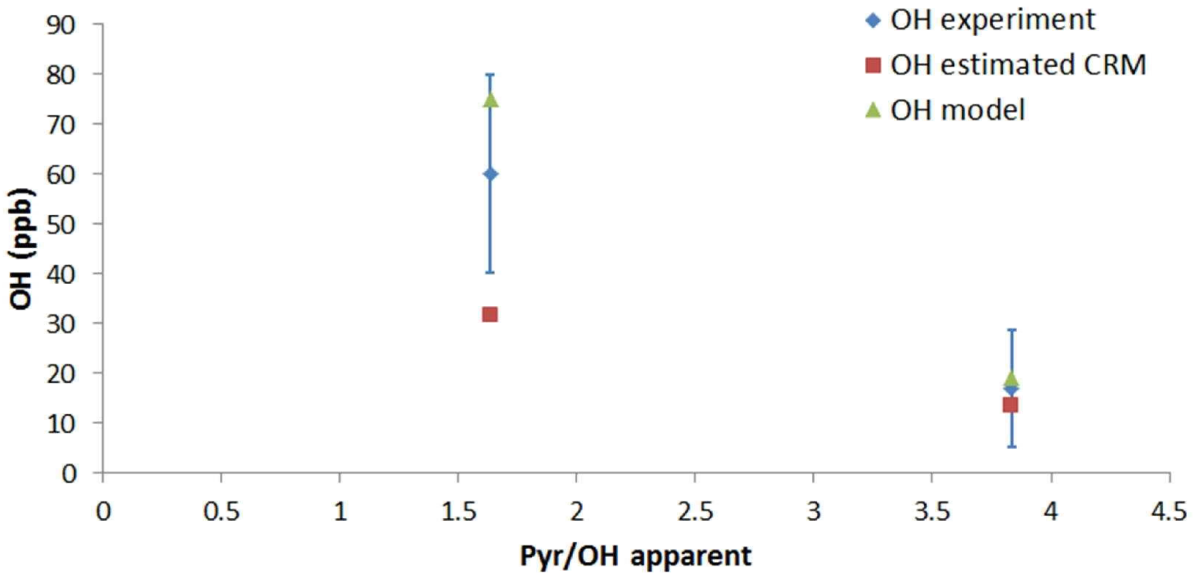

Figure S4: Comparison between OH mixing ratios determined experimentally ("OH experiment", blue diamonds), calculated from the C1-C2 modulation ("OH estimated CRM", red squares), and estimated from the model ("OH model", green triangles) at two different pyrrole-to-OH ratios (1.6 and 3.8). Error bars are the measurement precision. Large error bars (33-68%) are found since these OH measurements correspond to differences of tens of ppb for an initial mixing ratio of isoprene of approximately 3 ppm.

Supplementary material 5: Influence of humidity on the NO artifact – simulation results

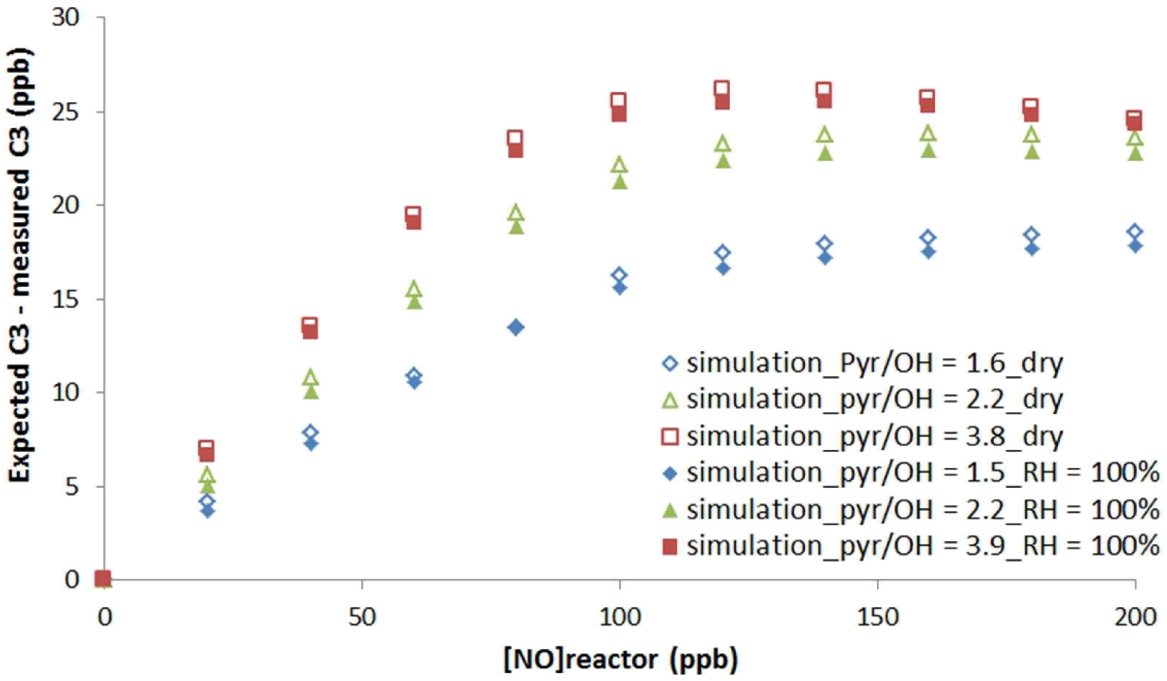

Figure S5: Comparison between simulations performed to investigate the NO artifact under dry (open symbols) and humid (filled symbols) conditions. These simulations were conducted at three different pyrrole-to-OH ratios of 1.5-1.6 (blue diamonds), 2.2 (green triangles), and 3.8-3.9 (red squares), using the simple mechanism and humid conditions corresponding to a relative humidity of 100%.

A small decrease of ΔC3 is observed at each pyrrole-to-OH ratio. This can be explained by an enhancement of the reaction rate of HO_2 + HO_2 in the presence of water, reducing the secondary formation of OH, hence the NO artifact.

Supplementary material 6: Influence of adding a gas standard on the NO artifact – simulation results

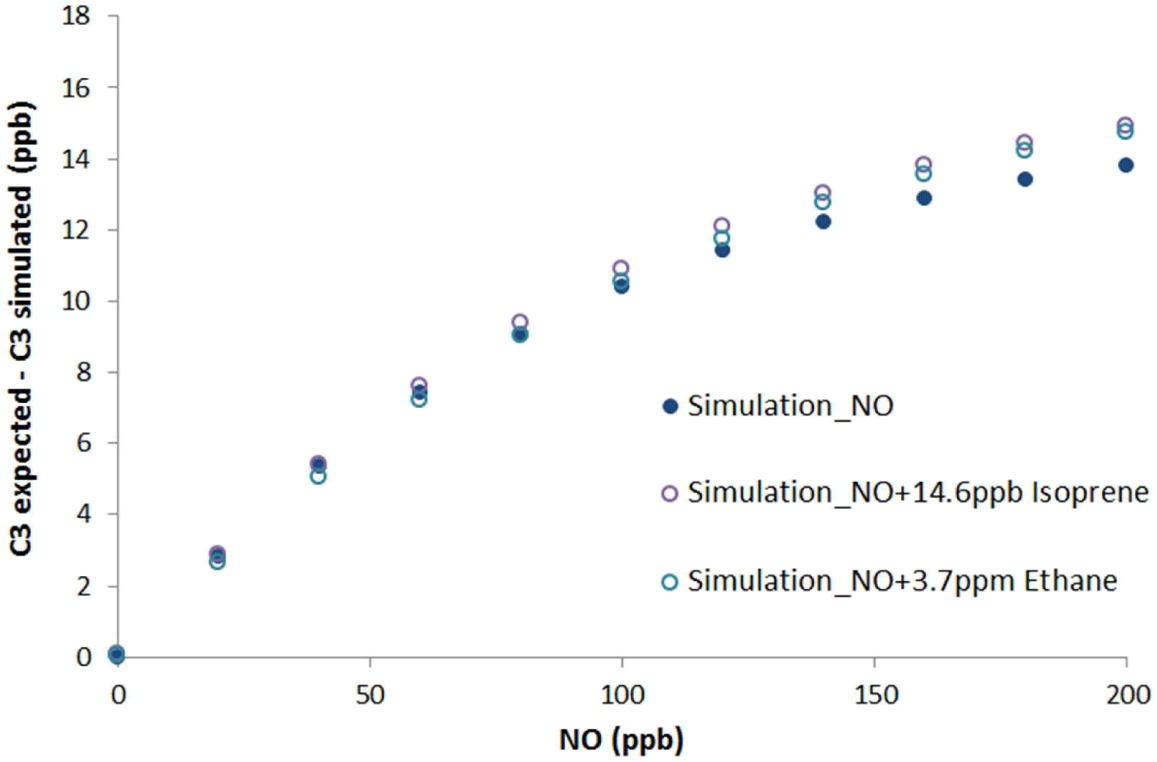

Figure S6: Simulated changes in C3 (ΔC3 = C3 expected – C3 simulated) as a function of NO. This figure shows simulations made with (open circles) and without (filled circles) adding a gas standard. These simulations were conducted with the MCM mechanism at a pyrrole-to-OH ratio of 1.4. The gas standards are isoprene (14.6 ppb) and ethane (3.7 ppm), leading to additional OH reactivities of 36.6 and 22.2 s^{-1}, respectively.

Supplementary material 7: Influence of the VOC bimolecular rate constant on the correction factor – experimental results

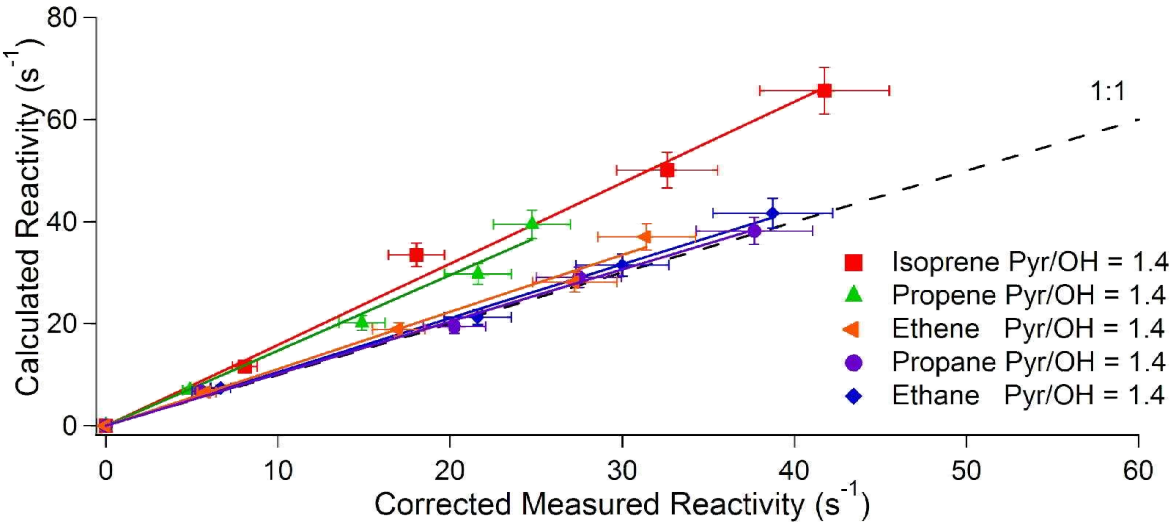

Figure S7: Experimental investigations of the bias caused by not operating the instrument under pseudo first-order conditions. Comparison of calculated (true) OH reactivity to CRM measurements during the addition of a gas standard into the reactor at a pyrrole-to-OH ratio of 1.4. Results from the addition of five different gas standards (Isoprene: red squares, Propene: green triangles, Ethene: orange triangles, Propane: purple circles, and Ethane: blue diamonds). These gas standards are characterized by reaction rate constants with OH of 1.0×0^{-10}, 2.9×10^{-11}, 8.5×10^{-12}, 1.1×10^{-12}, and 2.4×10^{-13} cm^3 $molecules^{-1}$ s^{-1}, respectively.

Supplementary material 8: Potential influence of reactant segregation on the simulations

One hypothesis to explain the differences observed between measurements and simulations for the bias caused by not operating the instrument under pseudo first-order conditions is a potential segregation of reactants coming from two different injectors (OH and HO_2 on one side and pyrrole + reactive trace gases on the other side). To account for this segregation (i.e. inhomogeneity in the reactor), we doubled the reaction rate constants of cross- and self-reactions of radicals (i.e. HO_2+OH and HO_2+HO_2), assuming that these reactions are favored by inhomogeneities inside the reactor since all the radicals are injected from the same injector. Figure S8 shows a comparison between base simulations and simulations including reactant segregation as a function of the pyrrole-to-OH ratio. Laboratory derived correction factors are also shown. These simulations suggest that segregation cannot explain the disagreement since a larger difference is found when compared to experimental observations.

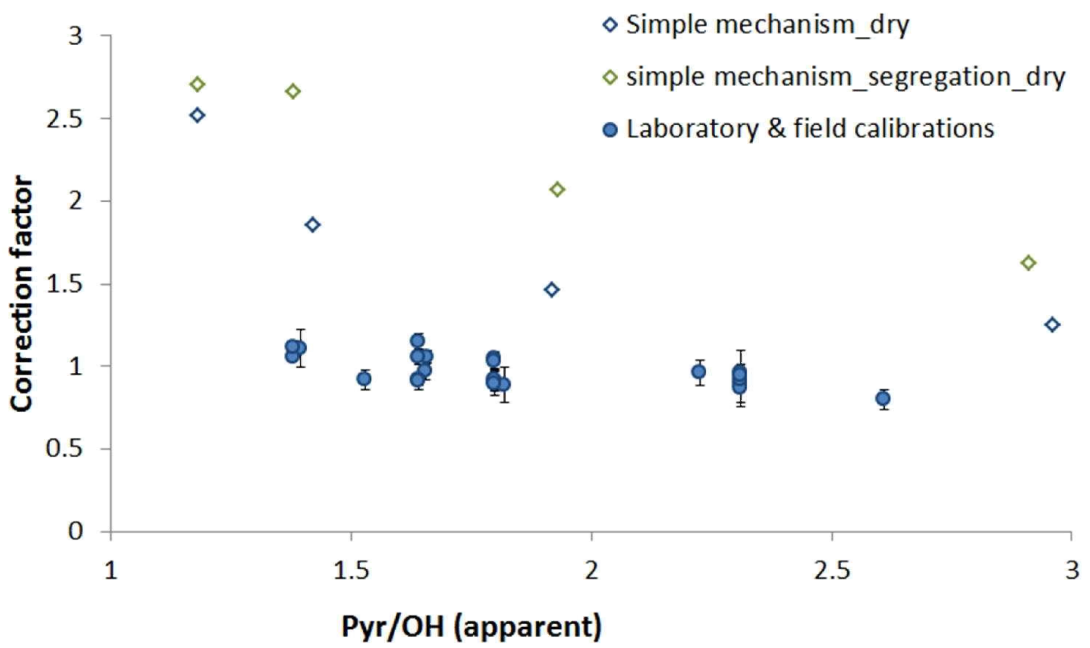

Figure S8: Comparison of simulated and measured correction factors required to correct for not operating the instrument under pseudo first order conditions. Correction factors are shown as a function of the Pyrrole-to-OH ratio. Measured correction factors (blues circles), as well as error bars, are the same than in Fig. 7. The simulated correction factors stem from simulations conducted using the simple mechanism (blue open diamonds) and the simple mechanism including the segregation effect (green open diamonds).

Supplementary material 9: Potential influence of RO_2+OH reactions on the simulations

A recent study has proposed the reaction of CH_3O_2 with OH as a potential sink of CH_3O_2 in the remote atmosphere (Fittschen et al., 2014). Since high radical concentrations are produced in the CRM reactor, radical-radical reactions may have an important impact on the CRM measurements. We have, therefore, tested the addition of the reaction between peroxy radicals and OH in the simple mechanism, assuming a reaction rate constant similar to the one of CH_3O_2 determined by Bossolasco et al. (2014). Figure S9 shows the comparison between the correction factors derived from base simulations and simulations including the fast RO_2+OH reactions as a function of the pyrrole-to-OH ratio. The addition of this reaction in the chemical mechanism leads to an increase of the correction factor and worsen the comparison.

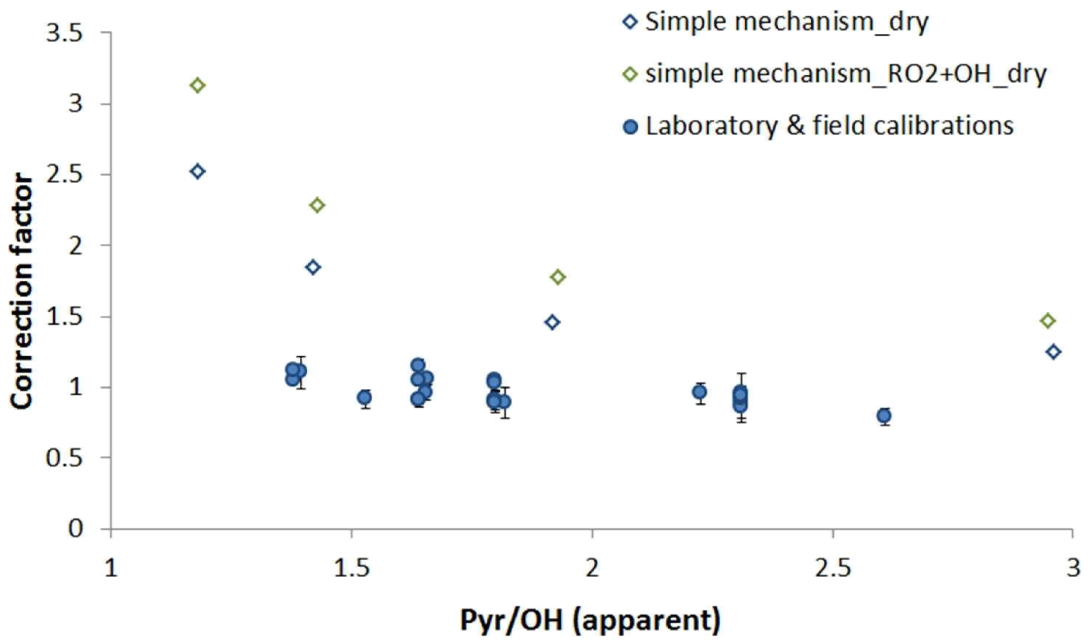

Figure S9: Comparison of the simulated and measured correction factors required to correct for not operating the instrument under pseudo first order conditions. Correction factors are shown as a function of the Pyrrole-to-OH ratio. Measured correction factors (blues circles), as well as error bars, are the same than in Fig. 7. The simulated correction factors stem from simulations conducted using the simple mechanism (blue open diamonds) and the simple mechanism including RO_2+OH reactions (green open diamonds). The reaction rate constant for RO_2+OH was set to 2.0×10^{-10} cm^3 $molecules^{-1}$ s^{-1}, corresponding to the rate constant of the reaction of CH_3O_2 + OH (Bossolasco et al., 2014).

Supplementary material 10: Potential influence of uncertainties associated to radical-radical reaction rate constants on the simulations

From the two previous tests (S8-S9), it appears that enhancing radical-radical reaction rates leads to an increase of the correction factors, which worsen the model-experiment comparison. One can imagine that an overestimation of reaction rate constants of these reactions can contribute to the discrepancies observed between measurements and simulations. To test the influence of uncertainties associated to radical-radical reaction rate constants, simulations were performed with a reduction of 20% and 50% of the reaction rate constant for HO_2+OH. Figure S10 shows the comparison between measured correction factors, base simulations, and simulations where a reduction of the reaction rate constant was made. This figure shows that a decrease of the HO_2+OH reaction rate constant allows to decrease the modeled correction factors and to get a better agreement with experimental observations. However, a reduction of the rate constant by 20% is not sufficient to reconcile measurements and simulations. Even a reduction of 50%, which is very unlikely, leads to simulated correction factors that are still slightly higher than the measurements. Therefore, the uncertainty of reaction rate constants of radical-radical reactions cannot totally explain the discrepancies between simulations and measurements.

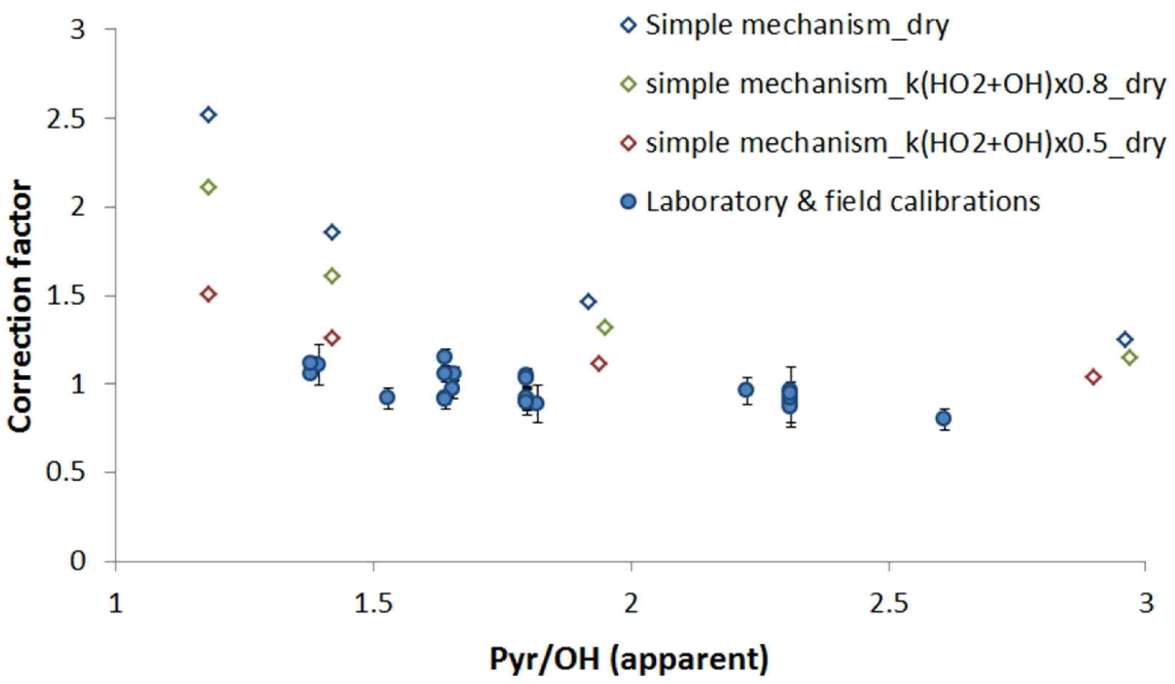

Figure S10: Comparison of the simulated and measured correction factors required to correct for not operating the instrument under pseudo first order conditions. Correction factors are shown as a function of the Pyrrole-to-OH ratio. Measured correction factors (blues circles), as well as error bars, are the same than in Fig. 7. The simulated correction factors stem from simulations conducted using the base simple mechanism (blue open diamonds) and the simple mechanism modified to reflect a slower reaction rate constant for HO_2+OH (green open diamonds: 20% reduction, red open diamonds: 50% reduction).

Supplementary material 11: Potential influence of a higher proportion of HO_2 compared to OH on the simulations

In all the simulations presented in the main paper and above, we assumed similar concentrations of HO_2 and OH since water photolysis produces similar amounts of these radicals. However, it is likely that a larger amount of OH radicals is lost on the walls of the injector compared to HO_2. Therefore, a HO_2–to-OH ratio higher than unity might be observed inside the reactor. The influence of a higher proportion of HO_2 compared to OH has been tested with the simple mechanism by setting initial HO_2 concentrations higher by 20% than OH concentrations.

Figure S11 shows the comparison between measured values, base simulations, and simulations where initial HO_2 concentrations are higher than initial OH concentrations by 20%. A higher proportion of HO_2 leads to higher simulated correction factors, which worsen the comparison.

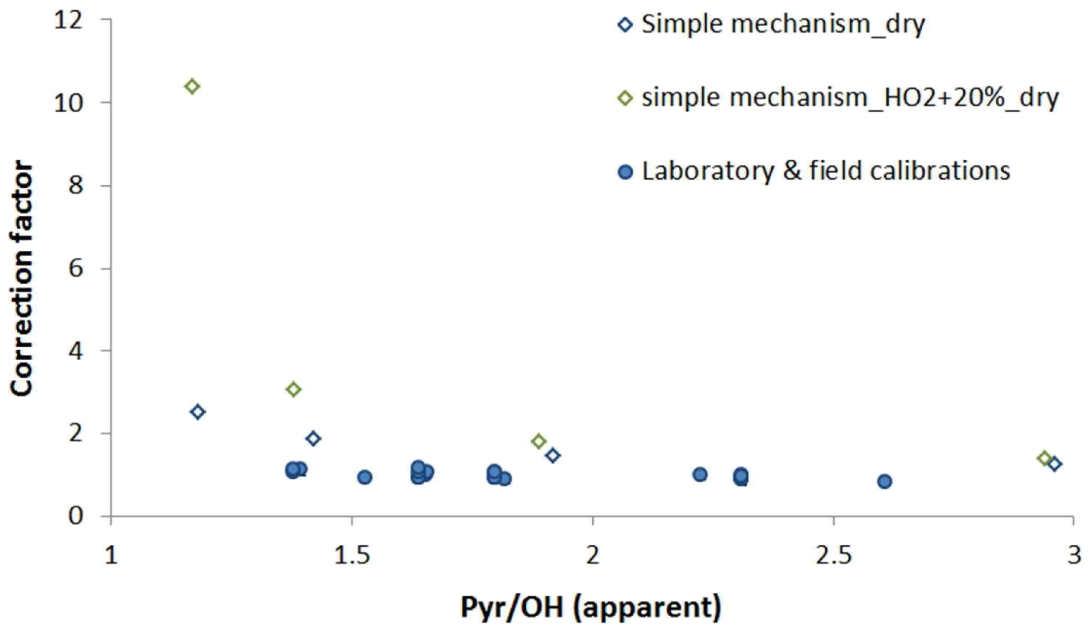

Figure S11: Comparison of simulated and measured correction factors required to correct for not operating the instrument under pseudo first order conditions. Correction factors are shown as a function of the Pyrrole-to-OH ratio. Measured correction factors (blues circles), as well as error bars (hardly visible), are the same than in Fig. 7. The simulated correction factors stem from simulations conducted using the simple mechanism assuming the same concentration for OH and HO_2 (blue open diamonds) and 20% more HO_2 than OH (green open diamonds).

Supplementary material 12: Potential influence of O_3 inside the reactor on the simulations

All the simulations presented in this work have been performed without O_3. However, photolysis of O_2 from the mercury lamp emission at 184.9 nm may occur inside the reactor and may lead to the formation of a significant amount of O_3. In this context, the influence of O_3 was tested for both the pseudo first order correction and the NO artifact. The O_3 mixing ratio was set at 200 ppb in the simulations, which corresponds to the mixing ratio measured using an ozone analyzer (Environnement-SA, model O3-42M) at the exhaust of the reactor under dry conditions and the mercury lamp ON.

Figure S12.1 shows the comparison between measured correction factors required to correct for not operating the instrument under pseudo first order conditions, base simulations, and simulations where initial O_3 mixing ratios were set to 200 ppb. This figure shows that the presence of O_3 has almost no impact on the simulated correction factors. This can be explained by the fact that the kinetic rate constant for the reaction between Pyrrole and O_3 is seven orders of magnitude lower than the rate constant for the reaction between Pyrrole and OH while initial mixing ratios of O_3 are only a factor 2.3 to 19 higher than initial OH mixing ratios. Furthermore, these simulations indicate that the impact of the $O_3 + HO_2 \rightarrow OH$ reaction has only a small impact on CRM simulations, probably due to a slow reaction rate, even with high mixing ratios of HO_2 (27-220 ppb) and O_3 (200 ppb) inside the reactor.

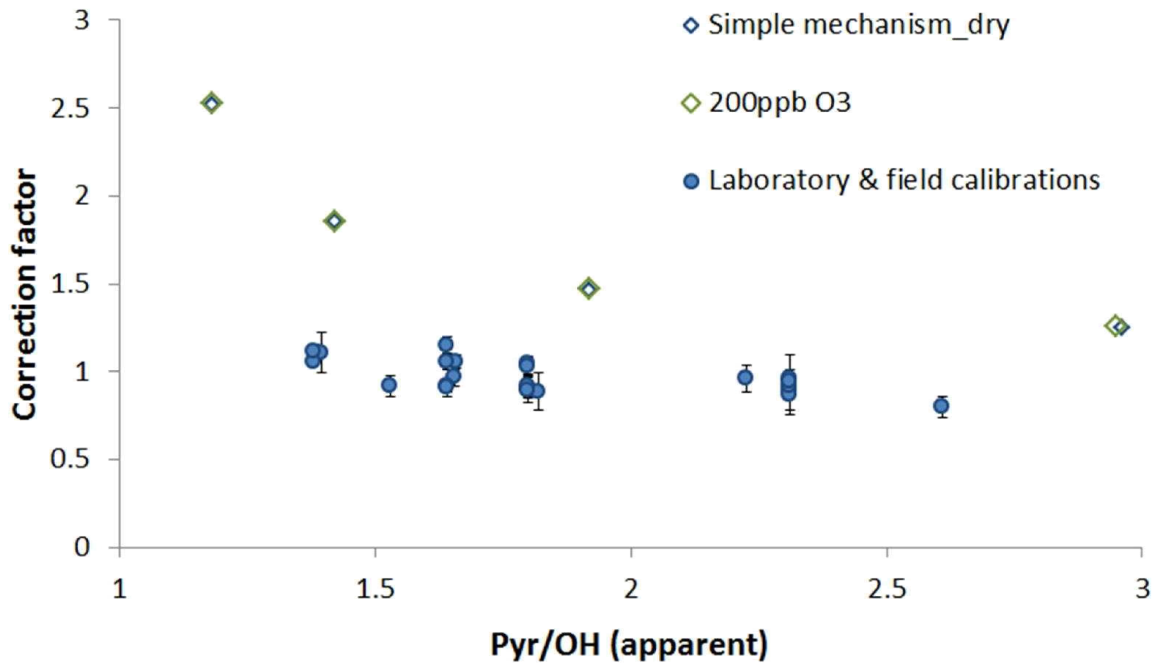

Figure S12.1: Comparison of simulated and measured correction factors required to correct for not operating the instrument under pseudo first order conditions. Correction factors are shown as a function of the Pyrrole-to-OH ratio. Measured correction factors (blues circles), as well as error bars, are the same than in Fig. 7. The simulated correction factors stem from simulations conducted using the base simple mechanism (blue open diamonds) and the simple mechanism where the initial mixing ratio of O_3 was set to 200 ppb (green open diamonds).

Figure S12.2 displays the comparison between experimental and simulated results for the NO artifact. Simulations were performed using the MCM mechanism and initialized with an O_3 mixing ratios of 200 ppb. This figure shows that the presence of ozone leads to a decrease of the NO artifact by approximately 2.5%, independent of the pyrrole-to-OH ratio.

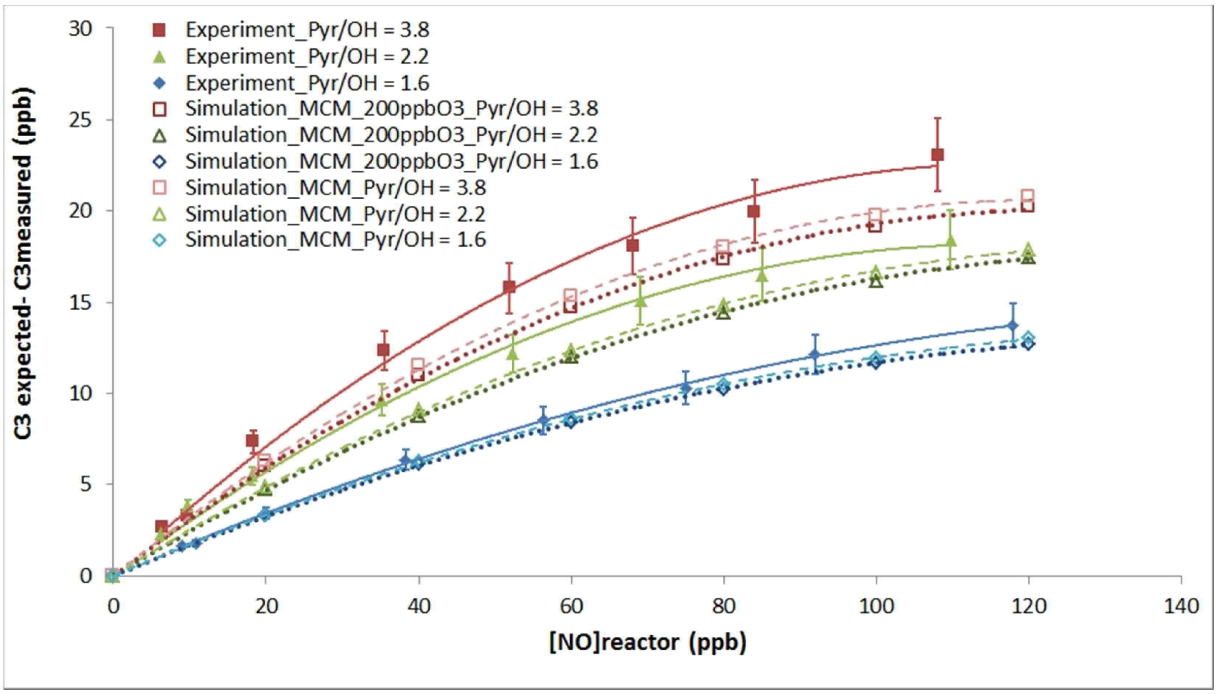

Figure S12.2: Comparison of laboratory observations to model simulations for the NO artifact. Experimental (filled symbols and solid lines) and simulated (open symbols and dashed or dotted lines) results are shown for the changes in C3 (ΔC3 = C3 expected – C3 measured) as a function of NO. Experimental values are the same than in Fig. 5. Model values are from simulations made using the base MCM mechanism (open lighter symbols and dashed lines) and the MCM mechanism where the initial O_3 concentrations was set to 200 ppb (open darker symbols and dotted lines).

Supplementary material 13: Potential influence of a lower proportion of HO_2 compared to OH on the simulations

As described in the supplement S12, a significant mixing ratio of O_3 (~200 ppb) is produced inside the reactor from the photolysis of O_2. Therefore, the ozone produced can lead to a production of OH inside the reactor from its photolysis ($O_3 + h\nu \rightarrow O^1D + O_2$ followed by $O^1D + H_2O \rightarrow 2OH$). This OH source is free of HO_2 production. If a non-negligible fraction of OH comes from this OH source, then the OH mixing ratio may be higher than HO_2. Therefore, the influence of a lower proportion of HO_2 compared to OH was also tested with the simple mechanism by setting initial HO_2 concentrations lower by 25% than OH concentrations.

Figure S13 displays the comparison between measured values, base simulations, and simulations where HO_2 concentrations were set lower by 25% than OH concentrations. This figure shows that a lower proportion of HO_2 leads to lower simulated correction factors. However, it cannot fully explain the discrepancies. Furthermore, a much lower proportion of HO_2 compared to OH is not likely since the photolysis of H_2O inside the injector will likely bring a larger amount of HO_2 compared to OH inside the reactor, which would partly balance the absence of HO_2 production from O_3 photolysis. It is worth noting that a reduction of HO_2 by 25% would also result in a reduction of the NO artifact by approximately 6% using the MCM mechanism (not shown).

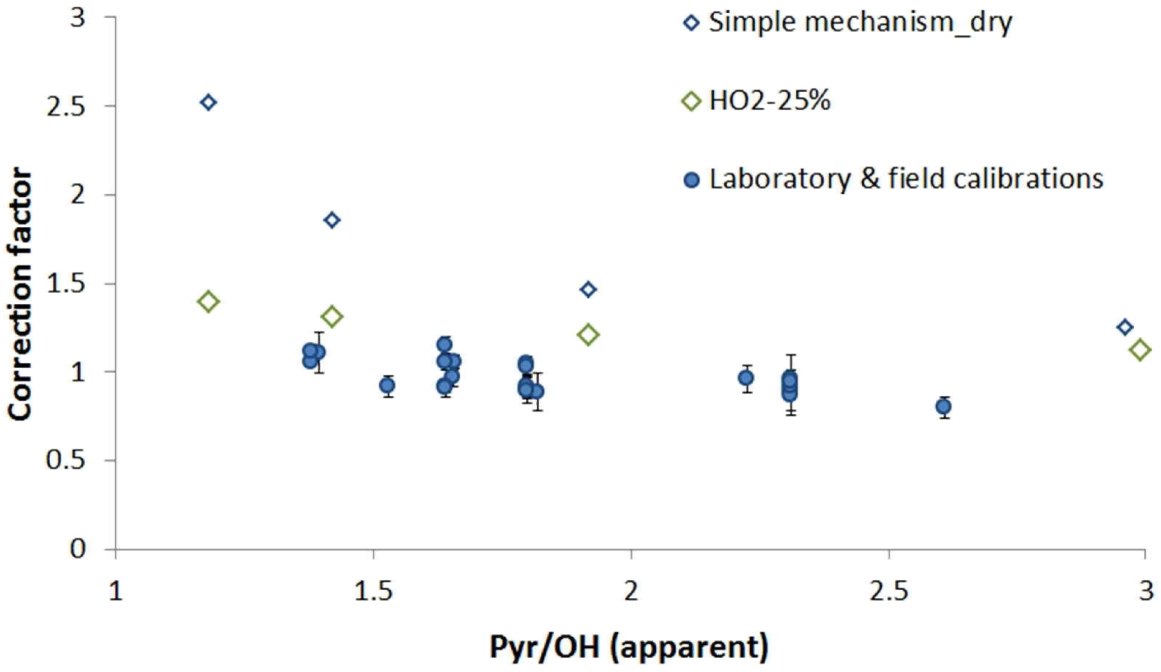

Figure S13: Comparison of simulated and measured correction factors required to correct for not operating the instrument under pseudo first order conditions. Correction factors are shown as a function of the Pyrrole-to-OH ratio. Measured correction factors (blues circles) as well as error bars are the same than in Fig. 7. The simulated correction factors stem from simulations conducted using the simple mechanism assuming the same concentration for OH and HO_2 (blue open diamonds) and a 25% lower proportion of HO_2 compared to OH (green open diamonds).

Supplementary material 14: Assessment of OH reactivity uncertainties

To assess the total uncertainty of ambient OH reactivity measurements it is necessary to take into account errors associated to each quantity involved in the OH reactivity calculations (Eq. 1), including the different corrections. When we account for the different corrections, the final OH reactivity is calculated by the following equation:

$$k_{OH} = \frac{((C3 + \Delta C3) - (C2 + \Delta C2)}{(C1 - (C3 + \Delta C3))} \cdot k_p.C1.F.D$$

Where k_{OH} is the final total OH reactivity, C3, C2 and C1 the concentrations of pyrrole at different measurement steps (see the main manuscript), ΔC3 the change in C3 due to the NO artifact, ΔC2 the change in C2 due to a difference in RH between C2 and C3, k_p the reaction rate constant of pyrrole with OH, F the correction factor to apply for not operating the instrument under pseudo first-order conditions, and D the correction factor for dilution of ambient air inside the reactor.

Considering that uncertainties are only due to PTR-MS measurements of pyrrole concentrations, the above equation can be rearrange to express it in terms of measured signals (only for uncertainty determinations and not for reactivity quantification):

$$k_{OH} = \frac{((S3+\Delta S3)-(S2+\Delta S2)}{(S1-(S3+\Delta S3))} \cdot k_p . \frac{S1}{(S_{m19}+X_r.S_{m37}).R_f}.F.D$$

Where, S3, S2, and S1 are the pyrrole signals recorded by the PTR-MS at m/z 68 during the different measurement steps, ΔS3 and ΔS2 the changes in pyrrole signals due to the NO artifact and changes in relative humidity, respectively, R_F the PTRMS sensitivity to pyrrole, S_{m19} and S_{m37} the signals at m/z 19 (H_3O^+) and m/z 37 ($H_3O^+(H_2O)$), respectively, and X_r the normalization factor accounting for the humidity dependence of the PTR-MS sensitivity (determined experimentally as described by Hansen et al. (2015)).

Making the assumption that the normalization of pyrrole signals by H_3O^+ and $H_3O^+(H_2O)$ does not bring additional errors, the terms producing uncertainties in the measurements are: S1, S2, S3, ΔS2, ΔS3, k_p, R_f, F, and D.

Assuming that these variables are independent, we can calculate the total uncertainty for OH reactivity measurements using the following equation:

$$U^2_{f(x1,\ldots,xn)} = \int_1^n \left[\left(\frac{\partial f}{\partial xi} \right)^2 .u^2_{xi} \right]$$

Applied to the total OH reactivity measurements, this gives the following equations:

$$U^2_{R_{air}} = \left[\frac{(S3+\Delta S3).[(S2+\Delta S2)-(S3+\Delta S3)]}{(S1-(S3+\Delta S3)^2} . \frac{1}{(S_{m19}+X_r.S_{m37})R_f} k_p.F.D \right]^2 .(\sigma^2_{S1})$$

$$+\left[\frac{-1}{(S1-(S3+\Delta S3)} . \frac{S1}{(S_{m19}+X_r.S_{m37})R_f} .k_p.F.D \right]^2 .(\sigma^2_{S2}+\sigma^2_{\Delta S2})$$

$$+\left[\frac{(S1-(S2+\Delta S2))}{(S1-(S3+\Delta S3)^2} . \frac{S1}{(S_{m19}+X_r.S_{m37})R_f} k_p.F.D \right]^2 .(\sigma^2_{S3}+\sigma^2_{\Delta S3})$$

$$+\left[\frac{(S3+\Delta S3)-(S2+\Delta S2)}{(S1-(S3+\Delta S3)} . \frac{S1}{(S_{m19}+X_r.S_{m37})R_f} F.D \right]^2 .(\sigma^2_{kp})$$

$$+\left[\frac{(S3+\Delta S3)-(S2+\Delta S2)}{(S1-(S3+\Delta S3)} . \frac{S1}{(S_{m19}+X_r.S_{m37})R_f} k_p.D \right]^2 .(\sigma^2_{F})$$

$$+\left[\frac{(S3+\Delta S3)-(S2+\Delta S2)}{(S1-(S3+\Delta S3)} . \frac{S1}{(S_{m19}+X_r.S_{m37})R_f} k_p.F \right]^2 .(\sigma^2_{D})$$

$$+\left[-\frac{(S3+\Delta S3)-(S2+\Delta S2)}{(S1-(S3+\Delta S3)} . \frac{S1}{(S_{m19}+X_r.S_{m37})R^2_f} k_p.F.D \right]^2 .(\sigma^2_{Rf})$$

Since the statistics for PTR-MS signals follow a poissonian distribution (De Gouw and Warneke, 2007): $\sigma_{S1} = \sqrt{S1}$, $\sigma_{S2} = \sqrt{S2}$, and $\sigma_{S3} = \sqrt{S3}$. These terms represent the random error (precision) of the PTR-MS measurements. To calculate the precision on OH reactivity

measurements, it is therefore possible to consider only these three uncertainties as non-zero in the above equations.

Terms leading to systematic errors are: k_p, R_f, F, and D. Their relative uncertainties (1σ) are described below:

- $\frac{\sigma_{kp}}{k_p}$ is estimated from the literature to be 8% (Dillon et al., 2012).
- $\frac{\sigma_{R_f}}{R_f}$ is calculated as the relative standard deviation of pyrrole calibrations performed during the campaigns and in the laboratory, and from the uncertainty on the pyrrole standard (1σ of 5%). $\frac{\sigma_{R_f}}{R_f}$ is estimated to be 12%.
- $\frac{\sigma_F}{F}$ is calculated from the standard deviation of correction factors obtained for different standards and within a restrained range of pyrrole-to-OH ratios (1.4-2.2) assuming that the pyrrole-to-OH dependence of F on this range of ratios is small. The corresponding relative uncertainty is 9%.
- $\frac{\sigma_D}{D}$ is calculated from uncertainties associated to different flow rates (PTR-MS sampling, reactor exhaust, addition of N_2 and pyrrole) that are controlled by mass flow controllers (estimated at 1%). The overall relative uncertainty to the dilution is estimated to be 2%.

Finally, uncertainties for ΔS3 and ΔS2 are given below:

- ΔS2 is calculated using the following equation: $\Delta S2 = p\left[\left(\frac{Sm37}{Sm19}\right)_{S3} - \left(\frac{Sm37}{Sm19}\right)_{S2}\right]$ (see equation (3) from the main manuscript), where p is the slope of the linear relationship observed between the pyrrole signal and the m37/m19 ratio. Since the uncertainty on the m37/m19 ratio is negligible (~0.05%), it is assumed that $\frac{\sigma_{\Delta S2}}{\Delta S2}$ depends only on the error associated to the slope and is estimated, from laboratory and field experiments, to be 12%.
- ΔS3 is calculated using a quadratic regression depending on NO: $\Delta S3 = a'.NO^2 + b'.NO$. The relative uncertainty for ΔS3 is estimated by propagating errors on the determinations of *a'* and *b'* and on the NO measurements:

  $$\frac{\sigma\Delta S3}{\Delta S3} = \sqrt{\left(\frac{U_{NOmeasurement}}{NO}\right)^2 + \left(U^{rel}_{parametrization}\right)^2}$$

  Errors associated to the determinations of *a'* and *b'* are estimated using the 1σ confidence intervals of the quadratic regression (see Fig. S14.1). These errors are found to be dependent on the NO mixing ratio.

The error on NO measurements is estimated using the specification given by the constructor for the NO_x analyzer (Thermo Environmental Instruments, model 42C), i.e. a limit of detection of 0.4 ppb, and a relative precision of 4% determined experimentally.

$$U_{NOmeasurement} = \frac{LOD}{3} + relative.precision \times NO$$

The overall relative uncertainty for this correction ($\frac{\sigma \Delta S3}{\Delta S3}$) regarding the NO mixing ratio is shown in Fig. S14.2.

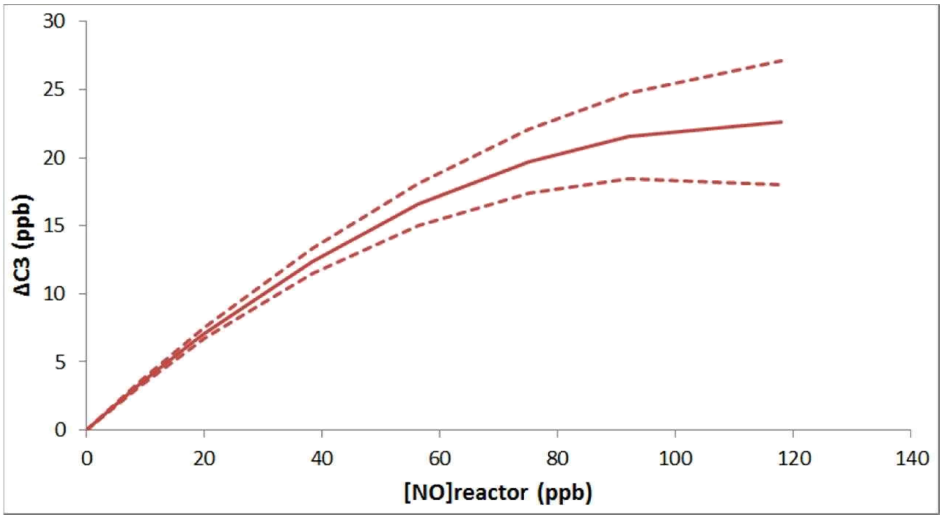

Figure S14.1: Change in C3 as a function of NO. The solid line corresponds to an estimated ΔC3 using the quadratic regression determined experimentally for a pyrrole-to-OH ratio of 3.8, for which the largest uncertainties are expected. The dashed lines display the 1σ confidence interval calculated using errors associated to *a'* and *b'*.

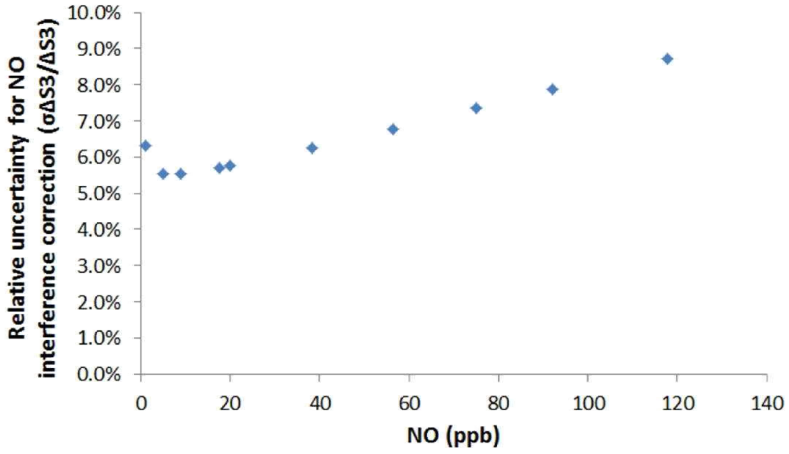

Figure S14.2: Trend of $\sigma\Delta S3/\Delta S3$ with NO. The relative uncertainty for this correction is estimated by propagating errors associated to the determinations of *a'* and *b'* (quadratic regression of ΔC3=f(NO)) and the measurement error on NO.

References

Bossolasco, A., Faragó, E. P., Schoemaecker, C., and Fittschen, C.: Rate constant of the reaction between CH_3O_2 and OH radicals, Chem. Phys. Lett., 593, 7–13, 2014.

De Gouw, J. and Warneke, C.: Measurements of volatile organic compounds in the Earth's atmosphere using proton-transfer reaction mass spectrometry, Mass Spectrom. Rev., 26, 223–257, 2007.

Dillon, T., Tucceri, M., Dulitz, K., Horowitz, A., Vereecken, L., and Crowley, J.: Reaction of Hydroxyl Radicals with C4H5N (Pyrrole): Temperature and Pressure Dependent Rate Coefficients, J. Phys. Chem. A., 116, 6051–6058, doi:10.1021/jp211241x, 2012

Fittschen, C., Whalley, L. K., Heard, D. E.: The Reaction of CH3O2 Radicals with OH Radicals: A Neglected Sink for CH3O2 in the Remote Atmosphere, Environ. Sci. Technol., 48, 14, 7700-7701, 2014

Hansen, R. F., Blocquet, M., Schoemaecker, C., Léonardis, T., Locoge, N., Fittschen, C., Hanoune, B., Stevens, P. S., Sinha, V., and Dusanter, S.: Intercomparison of the comparative reactivity method (CRM) and pump-probe technique for measuring total OH reactivity in an urban environment, Atmos. Meas. Tech. Discuss., 8, 6119-6178, doi:10.5194/amtd-8-6119-2015, 2015